Proceedings of the XXIII Conference on Applied Crystallography, Krynica Zdrój, Poland, September 20–24, 2015

Structure and Magnetic Properties of Amorphous $Fe_{60}Co_{10}Mo_2W_xY_8B_{20-x}$ ($x = 0, 1$) Alloys

K. Błoch*, M. Nabiałek and S. Garus

Częstochowa University of Technology, Institute of Physics, Faculty of Production Engineering and Materials Technology, al. Armii Krajowej 19, 42-200 Częstochowa, Poland

This paper presents studies of the bulk amorphous alloys: $Fe_{60}Co_{10}Mo_2Y_8B_{20}$ and $Fe_{60}Co_{10}Mo_2W_1Y_8B_{19}$; both compounds were obtained by means of the injection-casting method in which liquid alloy is forced under pressure into a copper mould. The structure of the samples was studied using X-ray diffraction and scanning electron microscopy. Based on the results of the X-ray diffraction studies, it was found that the samples were in the amorphous state. Scanning electron microscopy image analysis of fractured alloy samples indicated the presence of areas of varying degrees of relaxation: "smooth", "vein", and "flake" fractures. The manufactured ferromagnetic samples were characterized by so-called soft magnetic properties with a relatively high Curie temperature of more than 520 K. In the investigated samples, the saturation magnetization was found to have been decreased from 1.14 T to 1.13 T after the addition of W. Tungsten also contributed significantly to an increase in the value of the coercive field, from 27 A/m to 8685 A/m. Following the addition of just 1% of W to the alloy, a substantial change was observed in the form of the static magnetic hysteresis loop: characterized by the so-called "wasp" shape. This result shows that an additional magnetically hard phase had appeared within the sample.

DOI: 10.12693/APhysPolA.130.905

PACS/topics: 75.47.Np, 75.50.Bb, 75.50.Kj, 75.90.+w

1. Introduction

Modern materials with unique properties are highly sought after in industry. Commercially applied metal materials usually have a crystalline structure. However, in the 1950s, a new group of metallic materials was created, featuring amorphous structure [1]. Unfortunately, early materials were only available in the form of either thin-film layers or tapes of a few tens of μm; application of these samples was, and remains to be, difficult. Therefore, work was undertaken to develop methods and criteria for the systematic production of amorphous materials featuring larger thicknesses. After several decades, Inoue established new criteria, which, when applied, can lead to an amorphous alloy sample with a thickness in excess of 100 μm [2]. Since then, a number of bulk amorphous alloys have been created, along with modifications involving either heat treatment, slight changes in the chemical composition, or combinations of the two methods [3, 4].

The structure of amorphous materials is always seen as a collection of randomly arranged atoms and there are no descriptions of states of this structure, which can yield different properties. Often, within the volume of amorphous alloys there are several crystalline metastable phases, the detection of which is very difficult [5–7]. Typically, these phases are often trigonal, being composed of several tens of atoms that are distributed spatially at distances of up to 2 nm. In ferromagnetic alloys that are based on FeCoB, the predominant metastable phase is the $Fe_{23}B_6$ phase. However, changes in the properties of amorphous alloys are not always related to the recombination of their structure. Sometimes, there is poor mixing of the alloying elements during the manufacturing process, especially when hard elements with high-melting points (such as W) are added to the starting component elements. As demonstrated in the literature [8], the addition of 1 at.% tungsten can result in a significant improvement in the soft magnetic properties of an amorphous structure.

This paper presents the results of investigations into the structural and magnetic properties of the following pair of bulk alloys: $Fe_{60}Co_{10}Mo_2W_xY_8B_{20-x}$ (where $x = 0, 1$); the investigated samples were produced by an injection-casting process, in which the alloys underwent rapid-quenching within a copper mould.

2. Experimental procedure

This research was conducted on samples of the following alloys: $Fe_{60}Co_{10}Mo_2W_xY_8B_{20-x}$ (where $x = 0, 1$), which were prepared by injecting the molten alloy into a water-cooled copper mould. The alloy sample was obtained in the form of plate with dimension of $10 \times 10 \times 0.5$ mm^3.

In each case, the microstructure of the produced alloys was studied, using an X-ray diffractometer and a scanning electron microscope. The X-ray diffraction studies were carried out within the 2Θ-angle range of 30° to 100° with a step-size of 0.02°. For this purpose, an X-ray diffractometer from Bruker was used, equipped with a lamp with characteristic radiation type: Cu K_α and wavelength $\lambda = 1.54056$ Å. The microstructural studies were carried out using a Supra 35 high-resolution scanning electron microscope, manufactured by Zeiss. To obtain the images, secondary electron (SE) detection was used, with an accelerating voltage of 25 kV and maximum zoom (25,000×).

*corresponding author; e-mail: 23kasia1@wp.pl

The magnetic properties of $Fe_{60}Co_{10}Mo_2W_xY_8B_{20-x}$ (where $x = 0, 1$) were investigated using a Faraday balance and a vibrating sample magnetometer (VSM) with a magnetic field of up to 2 T; the magnetometer was made by LakeShore. Magnetic balance measurements were performed over the temperature range of 300 K to 850 K.

3. Results and discussion

Figure 1 shows the X-ray diffraction patterns obtained for the examined alloy plate samples of $Fe_{60}Co_{10}Mo_2W_xY_8B_{20-x}$ (where $x = 0, 1$) in the as-quenched state, following solidification in the water-cooled mould.

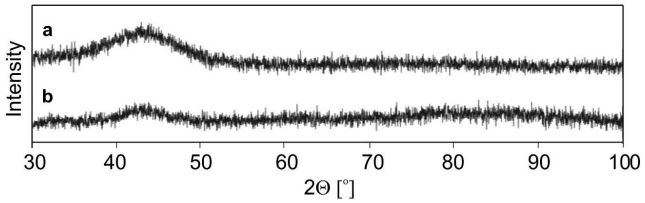

Fig. 1. XRD patterns of: (a) $Fe_{60}Co_{10}Mo_2Y_8B_{20}$ and (b) $Fe_{60}Co_{10}Mo_2W_1Y_8B_{19}$.

In the X-ray diffraction patterns, it can be seen that there are no narrow peaks typical of crystalline materials. The diffraction patterns obtained for these amorphous samples consist predominantly of a single broad peak, called the "amorphous Halo". X-ray radiation is scattered on randomly arranged atoms in the amorphous material, for which it is difficult to determine the unit cell constituting the pattern of the structure. Therefore, the effect of this X-ray scatter reflected from the amorphous sample is a wide diffuse peak of low intensity.

Figure 2 shows the SEM images of fractured samples of the alloys, displayed in the form of tiles.

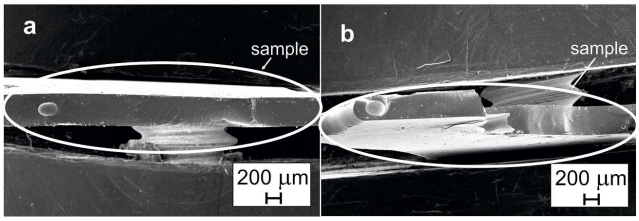

Fig. 2. SEM images of the investigated alloys: (a) $Fe_{60}Co_{10}Mo_2Y_8B_{20}$, (b) $Fe_{60}Co_{10}Mo_2W_1Y_8B_{19}$.

In fractures that are produced by decohesion, it can be seen that, for both alloys, there is a characteristic mixed fracture separated by a heterogeneous structure in the form of gas bubbles. The presence of this type of fracture is related to the solidification process of the material. The consolidation process of the investigated alloys does not occur uniformly throughout the whole volume, and this is the reason for the formation of the various structures, as evidenced by the observed fracture characteristics. SEM images for the $Fe_{60}Co_{10}Mo_2Y_8B_{20}$ alloy are shown in Fig. 3. Figure 3a indicates areas in which discontinuities have been formed in "vein ridges", changing them into "flake" shapes.

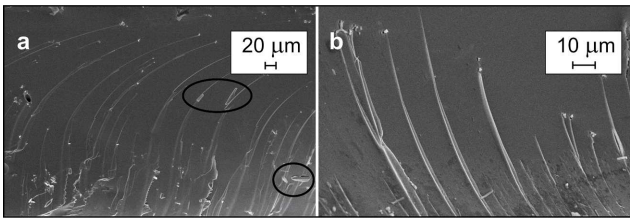

Fig. 3. SEM images of the alloy: $Fe_{60}Co_{10}Mo_2Y_8B_{20}$.

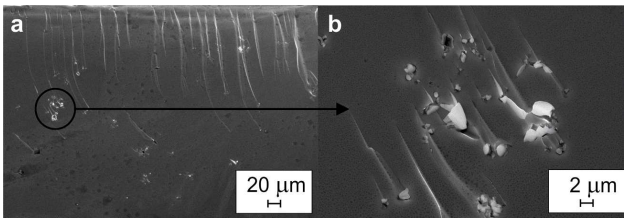

Fig. 4. SEM images of the alloy: $Fe_{60}Co_{10}Mo_2W_1Y_8B_{19}$.

For the sample of $Fe_{60}Co_{10}Mo_2Y_8B_{20}$, stratification was observed in the structure of the string and the formation of flake structures. Creation of flake structures was observed for a larger surface area of fracture (Fig. 3), which indicates that the investigated alloy has a higher ductility than the alloy sample containing tungsten (Fig. 4).

In the case of both samples, heterogeneities of the structure were observed, in the form of gas bubbles. In Fig. 5, an example of a gas bubble is shown for the alloy: $Fe_{60}Co_{10}Mo_2W_1Y_8B_{19}$ [7].

Due to the rapid solidification of the molten alloy, following its injection into the copper mould, gas bubbles are trapped within the volume of each sample. Therefore, the observed structure of the investigated alloys is very heterogeneous. Near the gas bubbles, the structure indicates variable local ductility of the alloy. In the amorphous alloys, the following three types of structures may be observed: smooth, vein and flake. In addition, a mixed structure can be observed in specific cases, or the "river" structure. From analysis of the fracture structure shown in Fig. 5, it can be concluded that the interior of the gas bubble is characteristic for the structure of a smooth fracture. This means that the solidification of the melt occurred relatively slowly near the trapped gas bubbles. In turn, this indicates that the most substantial relaxation of the alloy is in this area. Further away from the gas bubbles (an example of which is circled in Fig. 5) a vein structure is formed, and this is associated with improved ductility of the alloy. The addition of tungsten to the $Fe_{60}Co_{10}Mo_2Y_8B_{20}$ alloy produced a change in the fracture morphology (Fig. 4). In addition, within the volume of the alloy, regions can be found where there are concentrations of undissolved tungsten (Fig. 4a).

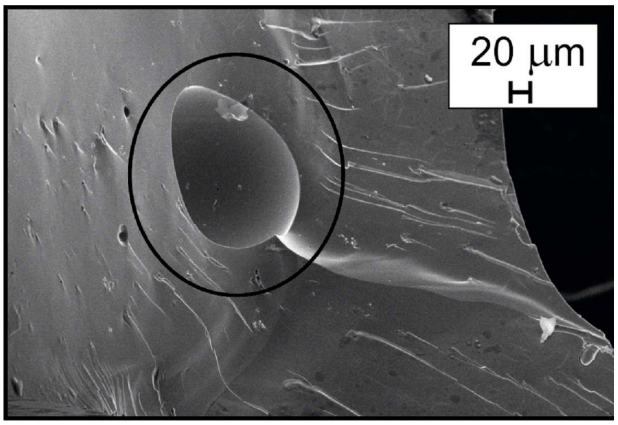

Fig. 5. Example of a gas bubble in the alloy: $Fe_{60}Co_{10}Mo_2W_1Y_8B_{19}$.

The addition of tungsten atoms to the $Fe_{60}Co_{10}Mo_2Y_8B_{20}$ alloy resulted in changes to the magnetic properties of the alloy.

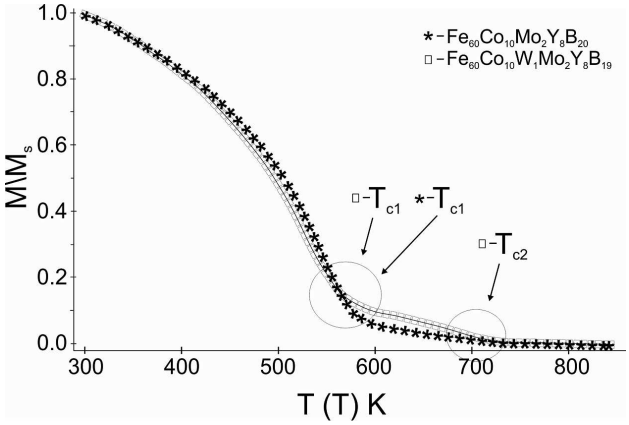

Fig. 6. Thermomagnetic curves pertaining to the investigated alloys.

Figure 6 shows thermomagnetic curves which were recorded for the investigated alloys. For the alloy: $Fe_{60}Co_{10}Mo_2Y_8B_{20}$, the shape of the thermomagnetic curve is typical for ferromagnetic materials with a single soft magnetic phase. In the case of the second alloy, a change was observed in the magnetic polarization (as a function of temperature). On the curve measured for the alloy $Fe_{60}Co_{10}Mo_2W_1Y_8B_{19}$, two inflections are visible, demonstrating the presence of two magnetic phases with relatively high Curie temperatures.

The presence of these two phases confirms the results derived from analysis of the static hysteresis loops (Fig. 7).

For the first of the investigated alloys, the shape of the static hysteresis loop is typical for ferromagnetic materials with soft magnetic properties. In the case of the $Fe_{60}Co_{10}Mo_2W_1Y_8B_{19}$ alloy, there is the so-called "wasp-like" shape of the hysteresis loop. It is believed that the broadening of the hysteresis loop is related to the

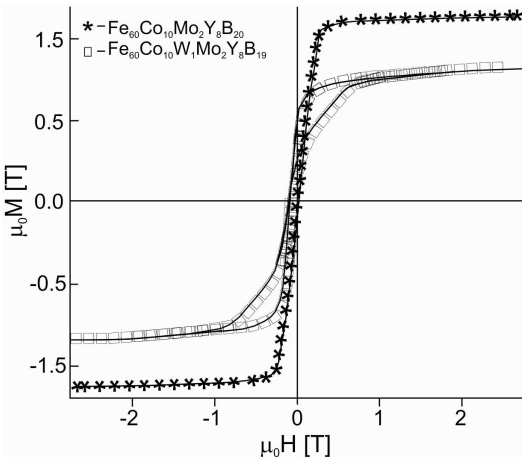

Fig. 7. Static hysteresis loops pertaining to the investigated alloys.

presence of the second magnetic phase (i.e. hard magnetic), which confirms the results obtained from the use of the Faraday magnetic balance. Data obtained from the analysis of the magnetic saturation polarization curves (as a function of the temperature) and the static hysteresis loops, are summarized in Table I.

TABLE I

The results obtained from analysis of the static hysteresis loops and thermomagnetic curves.

Parameters	$\mu_0 M_s$	H_c [A/m]	T_{C1} [K]	T_{C2} [K]
$Fe_{60}Co_{10}Mo_2Y_8B_{20}$	1.14	28	531	
$Fe_{60}Co_{10}Mo_2W_1Y_8B_{19}$	1.13	8685	522	675

4. Conclusions

Using the injection-casting technique, the following bulk amorphous alloys were obtained in the form of plates: $Fe_{60}Co_{10}Mo_2B_{20}$ and $Fe_{60}Co_{10}Mo_2W_1Y_8B_{19}$. The patterns obtained using X-ray diffraction were found to be typical for amorphous materials. Within fractures of the investigated samples, heterogeneity of the structure was observed — in the form of gas bubbles. In addition, it was found that the fractures were characterized by "smooth" and "vein" structures with a few "flakes". Undissolved tungsten clusters were observed in the SEM images obtained for $Fe_{60}Co_{10}Mo_2W_1Y_8B_{19}$. Both of the investigated alloys are magnetically soft ferromagnetics with relatively high Curie temperatures. Following the substitution of a boron atom with tungsten, an additional upward inflection (associated with the presence of the second magnetic phase) appeared in the thermomagnetic curve. For $Fe_{60}Co_{10}Mo_2B_{20}$, the Curie temperature is 531 K, while for the alloy containing tungsten, in which two magnetic phases have been detected, the Curie temperatures are 522 K and 675 K, respectively. The static hysteresis loop obtained for $Fe_{60}Co_{10}Mo_2W_1Y_8B_{19}$ is "wasp-shaped", which, according to [9, 10], testifies to

the existence of two phases: one being "very soft magnetic" and the other being "soft magnetic" [11]. It is very likely that, in a volume of alloy with added W, there are small clusters of crystallites whose detection using X-ray diffraction is impossible due to their low volume. It should also be noted that the magnetic saturation of the samples was comparable (Fig. 7), which means that the magnetic moment per unit volume was practically unchanged. Unfortunately, the introduction of 1 at.% of W in place of B had a large impact on the process of magnetization in the middle of the M–H characteristic and in the "approach to ferromagnetic saturation" area. As is known, the value of the coercive field depends on several factors: the domain structure, magnetoelastic interaction, magnetostriction and effective anisotropy. It is believed that undissolved clusters of tungsten cause heterogeneity in the alloy, blocking the free movement of domain walls in the volume of the alloy and representing centres for anchoring domain walls. In these systems, a local (as opposed to global) change is occurring in the prevailing type of magnetic interactions. In addition to the exchange interactions, dipole interactions also appear within the sample volume, and these are responsible for the increase in the value of the coercive field. It is believed that an appropriately conducted heat treatment process would lead to a sharp increase in the coercive field to the limits set by the peak broadening observed in the recorded static hysteresis loops.

References

[1] A. Inoue, *Material Science Foundations*, Vol. 6, TransTech Publ., 1998.

[2] A. Inoue, *Mater. Sci. Eng. A* **226–228**, 357 (1997).

[3] K. Błoch, M. Nabiałek, *Acta Phys. Pol. A* **127**, 442 (2015).

[4] S. Garus, M. Nabiałek, K. Błoch, J. Garus, *Acta Phys. Pol. A* **126**, 957 (2014).

[5] M. Stoica, R. Li, A. Reza Yavari, G. Vaughan, J. Eckert, N. Van Steenberge, D. Ruiz Romera, *J. Alloys Comp.* **504S**, 123 (2010).

[6] S. Lesz, R. Babilas, M. Nabiałek, M. Szota, M. Dośpiał, R. Nowosielski, *J. Alloys Comp.* **509S**, 197 (2011).

[7] B.L. Shen, H. Men, A. Inoue, *Appl. Phys. Lett.* **89**, 101915 (2006).

[8] J. Garus, S. Garus, M. Nabiałek, M. Szota, *Acta Phys. Pol. A* **126**, 954 (2014).

[9] J.C. Martinez-Garcia, J.C. Garcia, M. Rivas, *J. Non-Cryst. Solids.* **354**, 5123 (2008).

[10] M. Dośpial, J. Olszewski, M. Nabiałek, P. Pietrusiewicz, T. Kaczmarzyk, *Nukleonika* **60**, 15 (2015).

[11] M. Leonowicz, *Nanocrystalline Magnetic Materials*, WNT, Warszawa 1998 (in Polish).